seven-neighbor Born–von Karman general force model; k_c' is just the central ray solution $k'(0,0,0,0,0)$. The weighting factor F is

$$F=\exp\left(-\tfrac{1}{2}\left[\left(\frac{\theta}{\sigma_1}\right)^2+\left(\frac{\theta'}{\sigma_2}\right)^2+\left(\frac{\Delta k_0}{\sigma_3}\right)^2\right]\right)$$
$$\times\frac{\{(\mathbf{k}'-\mathbf{k}_0)\cdot\mathbf{e}(\mathbf{q})\}^2}{\omega^2}\frac{k'}{k_0}\frac{[1-\exp(-4.07k_0/k')]}{|J|},$$

where σ_1, σ_2, and σ_3 are experimental parameters describing the combined incident-beam angular divergence and sample mosaic spread, the scattered-beam angular divergence, and the incident wavelength spread in terms of assumed Gaussian shapes, respectively; the bracketed term gives an approximate representation of the wavelength dependence of the detector sensitivity; and the remaining terms arise from factors in the one-phonon differential scattering cross section. (We have ignored any variation of the Debye-Waller factor, which should be small here, and we have assumed equipartition of energy, which should be valid for the small wave-vector phonons for which the correction is important.)

For our experiment, $\sigma_1=0.01228$ rad, $\sigma_2=0.00818$ rad, and $\sigma_3/k_0=0.0329$. The correction appears to be important only for the shorter wave-vector phonons, the largest correction causing the ratio ν/q to be reduced approximately 5%. The correction almost always caused a reduction in the ratio ν/q. Where the second transverse branch is nearly degenerate with the low branch in the small q region, the correction had to be calculated for both branches and combined to yield the appropriate correction to the observed k'. Most of the numerical integrations were done for 3888 points in the five-dimensional space; rechecks of a number using a finer mesh involving 19 800 points showed the coarser calculation to be good to 10%.

PHYSICAL REVIEW VOLUME 177, NUMBER 3 15 JANUARY 1969

Magnetoacoustic Effect in Mercury†

Tommy E. Bogle,* Julian B. Coon,‡ and Claude G. Grenier
Department of Physics, Louisiana State University, Baton Rouge, Louisiana 70803

(Received 27 May 1968)

Geometric resonances in the ultrasonic attenuations have been observed in high-purity mercury single crystals with longitudinal sound waves propagated along five crystallographic directions at frequencies up to 165 MHz. Of the five, only data for the $(1\bar{1}0)$, (110), and $(11\bar{2})$ directions are reported. The dominant resonance branches have been assigned to calipers of the second-band electron-lens surface, with three major symmetry calipers being obtained. The remainder of the resonance branches have been assigned to orbits on the first-band hole surface. Various breakthrough dimensions of the hole surface were determined from these orbits. The pseudopotential coefficients corresponding to the planes bounding the first Brillouin zone in mercury have been estimated by comparing the geometric resonance data with the results of a four-pseudowave calculation neglecting spin-orbit coupling.

I. INTRODUCTION

The Fermi surface of crystalline mercury has been studied both experimentally and theoretically by a number of investigators in the past few years. The de Haas–van Alphen (dHvA) effect has yielded several extremal cross sectional areas[1]; extremal calipers of a portion of the surface have been determined from preliminary magnetoacoustic data[2]; effective masses on the Fermi surface have been determined from an Azbel-Kaner cyclotron resonance experiment[3]; and information about the topology has been obtained from magnetoresistance measurements.[4,5] The first theoretical determination of the band structure was a three plane wave pseudopotential calculation[1] based on the dHvA data. An empirical four parameter model[5] based on magnetoresistance data was later presented and used as a starting point, along with the dHvA data, for an eight plane wave pseudopotential calculation including spin orbit coupling and constrained to satisfy the requirement of compensation.[5] A detailed relativistic

---

† The financial assistance received from the Dr. Charles E. Coates Memorial Fund of the Louisiana State University foundation donated by George H. Coates for the preparation of this manuscript is gratefully acknowledged. Report No. ORO-3087-30 is prepared under U. S. Atomic Energy Commission Contract No. AT-(40-1)-3087. Part of this work was submitted by one of us (T.E.B.) as partial fulfillment of the requirements for the Ph.D degree in physics at Louisiana State University.

* Present address: Department of Physics, McNeese State College, Lake Charles, La.

‡ Present address: Department of Physics, University of Houston, Houston, Texas.

[1] G. B. Brandt and J. A. Rayne, Phys. Rev. **148**, 644 (1966).

[2] T. E. Bogle, C. G. Grenier, and J. M. Reynolds, Bull. Am. Phys. Soc. **2**, 183 (1967).

[3] A. E. Dixon and W. R. Datars, Solid State Commun. **3**, 377 (1965).

[4] W. R. Datars and A. E. Dixon, Phys. Rev. **154**, 576 (1967).

[5] J. M. Dishman and J. A. Rayne, Phys. Rev. **166**, 728 (1968).

TABLE I. Physical constants and crystallographic data for mercury.

Symbol	Value	Definition
$a_0{}^{a}$	2.9863 Å	Real space lattice vector at 5°K
g_0	2.3002 $Å^{-1}$	Reciprocal space lattice vector at 5°K
α	70°44.6′	Real space rhombohedral angle
β^{a}	104°21.7′	Reciprocal space rhombohedral angle at 5°K
Ω	22.996 $Å^{-3}$	Volume of unit cell in real space
k_F	1.3707 $Å^{-1}$	Free-electron Fermi radius
E_F	0.5261 Ry	Free-electron Fermi energy
ρ	14.48 g/cm³	Density extrapolated to 5°K
$X-U$	0.6345 $Å^{-1}$	See Fig. 1
$T-U$	0.6254 $Å^{-1}$	See Fig. 1
$L-U$	1.0337 $Å^{-1}$	See Fig. 1
$T-W$	0.7220 $Å^{-1}$	See Fig. 1
$X-K$	0.3611 $Å^{-1}$	See Fig. 1
$v_{1\bar{1}0}$	1.703×10^5 cm/sec	Longitudinal sound velocity in $(1\bar{1}0)$ direction
v_{110}	2.350×10^5 cm/sec	Longitudinal sound velocity in (110) direction
$v_{11\bar{2}}$	1.724×10^5 cm/sec	Longitudinal sound velocity in $(11\bar{2})$ direction
v_{111}	2.549×10^5 cm/sec	Longitudinal sound velocity in (111) direction
v_{100}	2.112×10^5 cm/sec	Longitudinal sound velocity in (100) direction

[a] Source: C. S. Barrett, Acta Cryst. **10**, 58 (1957).

augmented plane wave (RAPW) calculation[6] has been performed with the results yielding a surface topologically equivalent to that obtained from the plane wave calculations. All of these calculations yield a model in reasonable agreement with the above experiments with the following exceptions. The calculations predict cross sectional areas belonging to the second-band electron surface much too large to be in agreement with the experimentally observed values. Also both pseudopotential and RAPW calculations fail to predict correctly the angular extent of the experimentally observed open orbits as seen from the magnetoresistance data, whereas the four parameter model uniquely explains this angular range.

This work reports the results of a detailed magnetoacoustic experiment in an effort to gain a more precise knowledge of the Fermi surface of mercury.

II. STRUCTURE

The structure of crystalline mercury has been discussed extensively by a number of authors[1,3–6] and will only be summarized here along with the basic topological features of its Fermi surface.

Mercury is a divalent metal which crystallizes at approximately 223°K into a simple rhombohedral structure with one atom per unit cell. Lattice parameters, as well as other information pertaining to the crystal structure, are listed in Table I. The first Brillouin zone with symmetry points and principal symmetry axes labeled is shown in Fig. 1. The zone is composed of three distinct, inequivalent faces centered on X, T, and L, and perpendicular to the {110}, {111}, and {100} directions, respectively. In the discussion of the experimental results which follow, it will be necessary to refer to directions with respect to both the real and reciprocal lattice. The notation introduced by previous authors[1,6] will be adopted in which $[lmn]$ represents a direction with respect to the real lattice, while (lmn) refers to a direction with respect to the reciprocal lattice. It should be noted that the three orthogonal real space directions, [111], $[11\bar{2}]$, and $[1\bar{1}0]$, specify the same directions as the corresponding reciprocal lattice directions (111), $(11\bar{2})$, and $(1\bar{1}0)$. A plane or face perpendicular to the (lmn) direction is also referred to as a (lmn) plane or face. Similarly a $[lmn]$ plane would refer to a plane perpendicular to the $[lmn]$ direction.

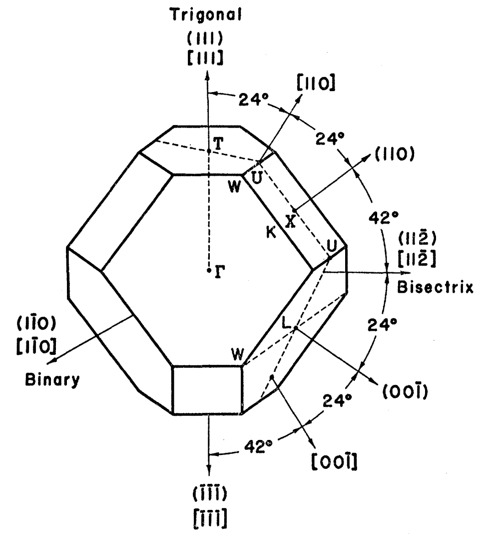

FIG. 1. The Brillouin zone for mercury.

Previous experiments and calculations are in essential agreement with a Fermi surface consisting of a double convex, lens shaped, second-zone electron disk centered at L on each of the six {100} faces bounding the first zone, and a multiply connected first-zone hole surface. The electron lenses are due to an overlapping of Fermi spheres from adjacent zones along the line Γ-L. The first-zone hole surface gives rise to a number of closed orbits along with several sets of open orbits. Experimental data and theoretical calculations indicate regions of contact between the Fermi sphere and the zone boundary at the points X and T in addition to L. This contact produces breakthrough regions, i.e., openings in the hole surface at these points. These openings allow for the existence of several additional closed orbits on the hole surface in addition to restricting the angular range of the open orbits.

---

[6] S. C. Keeton and T. L. Loucks, Phys. Rev. **152**, 548 (1966).

III. EXPERIMENT

The samples used in this investigation were prepared from high purity (99.99999%) mercury obtained from the United Mineral and Chemical Company.[7] Single crystals approximately 3.2 mm in thickness, with two smooth, flat, parallel surfaces, were grown using a modified Bridgeman technique. This involved lowering the sample mold filled with liquid mercury slowly into a dry-ice–methyl-alcohol bath at the rate of three inches per hour. Several single crystals were prepared in this manner and six were chosen for investigation with the normal to the parallel surfaces directed along the $(1\bar{1}0)$, (110), $(11\bar{2})$, [110], (111), and (100) crystallographic directions, respectively. The orientation of each sample was determined to within ±1° using standard x-ray techniques. Prior to being x-rayed, each sample was electropolished in a solution of 1% by volume of perchloric acid and 99% methyl alcohol at dry-ice temperatures.[8] This served a twofold purpose in that any surface damage to the crystals was removed rendering better x-ray photographs, and it indicated whether or not the sample was a single crystal immediately since any grain boundaries were revealed. All the samples were stored in liquid nitrogen between runs.

Due to the high attenuation of ultrasound in mercury, a dual transducer pulse transmission technique similar to that described by Kamm and Bohm[9] was employed to observe and record the geometric resonance signals. The electronic equipment used was identical to that described by Coon *et al.*[10] with the addition of two wideband amplifiers cascaded in front of the receiver to provide additional gain. A Z-cut quartz delay rod was used to delay the received pulse for 5 μsec in order to allow the receiver to recover sufficiently from the initial transmitter pulse which was capacitively coupled to the receiver. X-cut, gold plated, $\frac{1}{4}$-in.-diam quartz transducers with a fundamental frequency of 15 MHz were excited at an odd harmonic of the fundamental to generate and receive longitudinal sound waves. The receiving transducer was bonded to the delay rod with General Electric 7031 varnish and allowed to dry for two days before each run. The generating transducer and the delay rod were bonded simultaneously to the mercury sample immediately prior to each run using a mixture of 5 parts high-purity isopentane and 1 part 3-methylpentane. A small quantity of magnesium sulphate was added to both the isopentane and the 3-methylpentane in order to remove any water that may have been absorbed. This bonding arrangement was found to be satisfactory in most cases yielding a strong transmission pulse down to liquid-helium temperatures.

All data were taken at 1.2°K in order to reduce scattering due to thermal phonons. Since mercury is a superconductor at 1.2°K with a critical field of 360 G, it was necessary that the data be taken in magnetic fields in excess of this value. The magnetic field was set initially just below the critical value and swept such that H^{-1} was a linear function of time, yielding geometric resonances periodic in time, thereby simplifying the data analysis.

The velocities of propagation of longitudinal sound waves along the various crystallographic axes were determined experimentally. They were measured at 1.2°K and are tabulated in Table I. A detailed description of the determination of the velocity of sound along with the elastic constants of mercury will be reported elsewhere.

IV. THEORY AND DATA ANALYSIS

The general theory of magnetoacoustic attenuation in metals has been given by Cohen, Harrison, and Harrison[11] and by Pippard.[12] For the case of geometric resonances, it was found that the attenuation coefficient is periodic in the reciprocal of the magnetic field and that this period can be related to C, the k-space caliper of an electron orbit on the Fermi surface.

For the standard geometry in which the magnetic field $\mathbf{H}$ is rotated in a plane perpendicular to the direction of the sound propagation $\mathbf{q}$, the relation for the k-space caliper can be expressed as

$$C = \lambda e/\hbar c \Delta(1/H), \tag{1}$$

where C is twice the "radial caliper" of the Fermi surface in the direction $\hat{q}\times\hat{H}$, λ is the sound wavelength, and $\Delta(1/H)$ is the period of the oscillations in reciprocal field. The necessary condition for observing a series of geometric resonances is that $ql \gg 1$ and $\omega_c\tau > 1$, where $\mathbf{q}$ is the sound wave vector, l is the electron mean free path, ω_c is the cyclotron frequency, and τ is the characteristic scattering time for the electrons. The condition $\omega_c\tau > 1$ requires that an electron complete at least one real space orbit before being scattered, while $ql \gg 1$ requires that the completed orbit encompass several sound wavelengths. In the case of mercury, this latter condition could be satisfied for quite reasonable ultrasonic frequencies.

The assumption is generally made that C measures the extremal projection of the Fermi surface in the direction $\hat{q}\times\hat{H}$. However, Pippard[12–14] has indicated

---

[7] United Mineral and Chemical Corp., 16 Hudson Street, New York, N. Y.

[8] R. G. Goodrich (private communication).

[9] G. N. Kamm and H. V. Bohm, Rev. Sci. Instr. 33, 957 (1962).

[10] Julian B. Coon, Claude G. Grenier, and Joseph M. Reynolds, J. Phys. Chem. Solids **28**, 301 (1967).

[11] M. H. Cohen, M. J. Harrison, and W. A. Harrison, Phys. Rev. **117**, 937 (1960).

[12] A. B. Pippard, Proc. Roy. Soc. (London) **A257**, 165 (1960).

[13] A. B. Pippard, in *The Fermi Surface*, edited by W. A. Harrison and M. B. Webb (John Wiley & Sons, Inc., New York, 1960), p. 230.

[14] A. B. Pippard, in *Low-Temperature Physics*, edited by C. De Witt, B. Dreyfus, and P. G. de Gennes (Gordon and Breach Science Publishers, Inc., New York, 1962), p. 124.

that a limited series of oscillations may arise from regions which are not extremal if these regions couple strongly to the sound wave.

As has been pointed out,[15] extremal calipers can be uniquely converted into radius dimensions of the Fermi surface only if the given Fermi surface sheet has sufficient symmetry so that a set of extremal calipers measured on it for different directions of **H** all occur in a common plane about a common center. This occurs if a given sheet of the Fermi surface has both reflection symmetry in a plane perpendicular to **q** and inversion symmetry about some point in that plane.

It is advantageous at this point to briefly discuss the meanings of the terms extremal orbit and extremal caliper. An orbit is the intersection of the Fermi surface with a plane, $k_H=$ constant, perpendicular to **H**. The set of all possible calipers of the orbit may be obtained by measuring the normal distances between tangents to the orbit which are parallel to **q**. An extremal orbit as used in geometric resonance refers to an orbit which has a caliper that remains stationary with respect to small changes in k_H. The caliper for which an orbit is extremal is referred to as an extremal caliper of the Fermi surface.

Throughout this paper a system of notation similar to that of Ref. 15 will be adopted. The measured calipers will be reduced to radii whenever allowed by symmetry and will be denoted by the symbol k with a superscript to identify the direction and a subscript to identify the particular surface. For example, $k_{\text{lens}}{}^{L-\Gamma}$ refers to the radial caliper of the lens measured from L toward Γ. Calipers obtained from orbits not having sufficient symmetry to permit a reduction to radii will be denoted by the symbol C with an equivalent notation. Radial calipers will hereafter be referred to as k calipers while diametral calipers will be referred to as C calipers, i.e., a C caliper is twice a k caliper where allowed by symmetry. It will be assumed that all calipers presented here are due to extremal orbits unless otherwise specified.

Experimental extremal calipers were calculated using Eq. (1). The periods, $\Delta(1/H)$, were determined from the experimental data using a relation of the form

$$1/H_n=\Delta(1/H)(n+\gamma)\,, \qquad (2)$$

where n is the resonance number, and γ is a phase factor which is a function of n for small n but rapidly approaches a constant value as n increases. Since the attenuation theoretically reaches a relative maximum at integral values of n and a relative minimum at half integral values, γ can be determined from a plot of $1/H_n$ versus n with the best straight line fit through these points extrapolated to $1/H_n=0$.

For low magnetic fields such that the extremal dimension of an orbit is much longer than the wavelength λ, the resonances are strictly periodic in H^{-1}. This corresponds to the high-phase region and occurs for large values of n. The low-phase region occurs when the magnetic field is high enough such that λ is a significant fraction of the orbit diameter. The phase of the oscillations then shifts from its low-field asymptotic value and the oscillations are no longer strictly periodic in H^{-1}. Deviations from the H^{-1} periodicity occurring in the low-phase region are thus easily detected.

A knowledge of the phase is useful in identifying the oscillations and can yield information about the nature of the surfaces responsible for them. Theoretical considerations[16] indicate that $\gamma=0.25$ for a circular cylinder and $\gamma=0.375$ for a spherical surface. The data obtained for the lens surface of mercury yielded a value of $\gamma=0.27\pm0.07$.

V. EXPERIMENTAL RESULTS AND DISCUSSION

A. Electron Surface

1. Results for **q** *Parallel to the* (1$\bar{1}$0) *Direction*

Figure 2 presents a summary of all the C calipers obtained from data in the (1$\bar{1}$0) plane; **q** is in the (1$\bar{1}$0) direction, while θ measures the angle of the caliper direction from the trigonal axis. A total of ten distinct resonance branches were observed with each of the branches being designated with a Greek letter. Of these ten resonance branches, two, namely α_1 and α_2, have been assigned to the second-band electron surface.

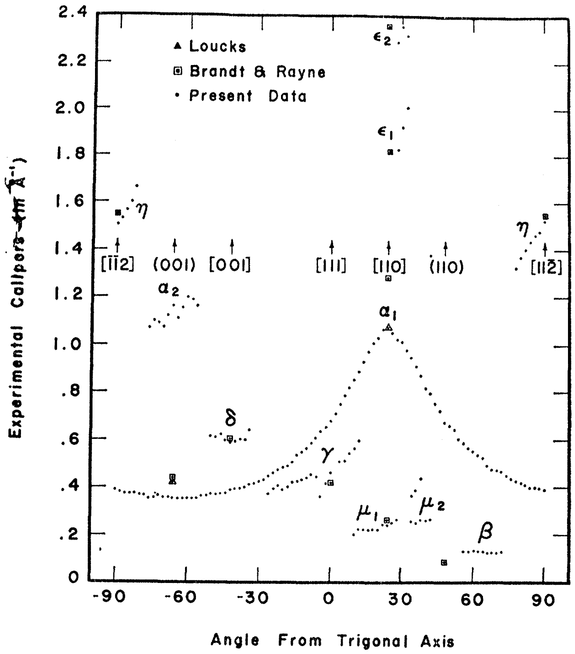

FIG. 2. A plot of all C calipers obtained for **q** parallel to the (1$\bar{1}$0) direction. Dimensions taken from Brandt and Rayne's dHvA-3PW calculation are shown for comparison as are the dimensions due to Loucks. All data were taken at 165 MHz.

---

[15] See, for example, J. B. Ketterson and R. W. Stark, Phys. Rev. **156**, 748 (1967).

[16] G. N. Kamm and H. V. Bohm, Phys. Rev. **131**, 111 (1963).

The resonances associated with the α_1 branch had the largest amplitude and have been assigned to calipers of a cross section of the second-zone electron-lens surface centered on the point L_1 in the $(1\bar{1}0)$ plane. The corresponding k caliper data for α_1 is shown on a polar plot in Fig. 3, along with a projection of the Brillouin zone on the $(1\bar{1}0)$ plane with the free-electron lenses sketched in for comparison. For notation purposes, the center of the lenses are denoted as L_1, L_2, and L_3. The errors presented refer only to uncertainties in the determination of the periods. The extremal dimensions of the cross section centered on L_1 have been found to differ slightly from the values previously reported[2] due to a small misorientation of the crystal from which the original data were taken. The results of the present data indicate a value for the minimum radius, $k_{\mathrm{lens}}{}^{L-\Gamma}$, of 0.176 ± 0.004 Å^{-1} and a value for the maximum radius, $k_{\mathrm{lens}}{}^{L-U}$, of 0.538 ± 0.010 Å^{-1}, whereas the values reported initially were $k_{\mathrm{lens}}{}^{L-\Gamma}=0.180$ Å^{-1} and $k_{\mathrm{lens}}{}^{L-U}=0.565$ Å^{-1}, respectively. Loucks[17] has reported dimensions obtained from his RAPW calculation of $k_{\mathrm{lens}}{}^{L-\Gamma}=0.215$ Å^{-1} and $k_{\mathrm{lens}}{}^{L-U}=0.540$ Å^{-1}, thus providing excellent agreement on the value of $k_{\mathrm{lens}}{}^{L-U}$. The cross sectional area of this section of the lens was determined graphically and found to be 0.299 Å^{-2} which is in good agreement with the value of 0.305 Å^{-2} determined by Brandt and Rayne from dHvA data. A comparison of the extremal areas of this cross section, along with the major and minor calipers as determined by different methods, is shown in Table II. This table includes the results of a 4 pseudowave (4 PW) calculation to be discussed later.

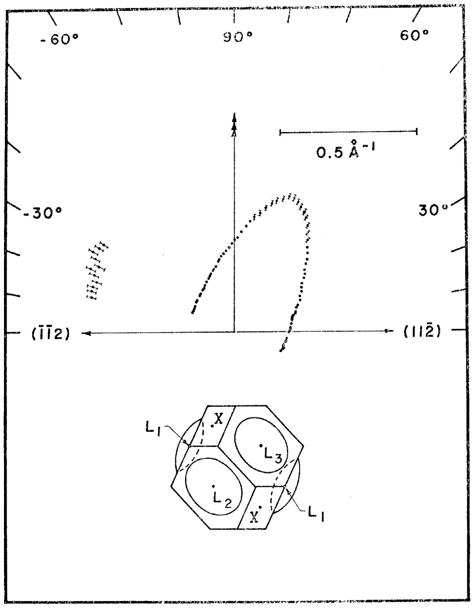

FIG. 3. A polar plot of data with **q** in the $(1\bar{1}0)$ direction. A projected view of the Brillouin zone in the $(1\bar{1}0)$ direction is shown along with a sketch of the free-electron lenses. The data were taken at a frequency of 165 MHz.

The C calipers designated α_2 in Fig. 2 have been assigned to a projection of one of the electron lenses onto the $(1\bar{1}0)$ plane. This projection is shown centered on the point L_2 or L_3 on the zone projection in Fig. 3. Resonances corresponding to these calipers were observed over an interval of about 22° in the vicinity of the (001) direction. The C calipers ranged from a value of 1.08 ± 0.04 Å^{-1} to 1.20 ± 0.02 Å^{-1} with considerable scatter in the data. The corresponding k caliper values are also shown in polar plot in Fig. 3.

2. *Results for* q *Parallel to the (110) Direction*

Figure 4 shows a polar plot of the data for **q** in the (110) direction and **H** rotated in the (110) plane. A projection of the Brillouin zone onto the (110) plane with the free-electron lenses sketched in for comparison is shown in the same figure. Only two distinct resonance branches were observed for this orientation as a result of the complete domination of the signal by resonances due to the lens. One branch was assigned to the projection of the lens centered on L_2 onto the (110) plane with the remaining branch being assigned to a similar projection of the lenses centered on L_1 and L_3. It should be noted that for perfect alignment of the sample, the projections of the surfaces centered on L_1 and L_3 should be identical if the lenses are surfaces of revolution about the Γ-L line.

TABLE II. Comparison of calipers and areas of lens obtained by different methods in $(1\bar{1}0)$ plane.

Source	$k_{\mathrm{lens}}{}^{L-\Gamma}$ (Å^{-1})	$k_{\mathrm{lens}}{}^{L-U}$ (Å^{-1})	Area (Å^{-2})
Free electron	0.220	0.730	0.441
dHvA 3PW[a]	0.204	0.600	0.344
8PW[b]	0.22	0.64	0.423
RAPW[c]	0.215	0.540	0.354
dHvA			0.305
Present calculation	0.176	0.540	0.300
Present experiment	0.176	0.538	0.299

[a] See Ref. 1.
[b] See Ref. 5.
[c] See Ref. 17.

With the magnetic field directed along the [001] direction, the maximum caliper of the projection of the surface centered on L_2 was found to have a value of $C_{L_2}{}^{0°}=1.28\pm0.03$ Å^{-1}. This caliper corresponds to the remaining symmetry axis caliper not obtained from the $(1\bar{1}0)$ data.

With the magnetic field in the $(\bar{1}10)$ direction, the minimum caliper of the projection of the lens centered on L_2 was found to be $C_{L_2}{}^{90°}=0.52\pm0.01$ Å^{-1}. A consistency check of this dimension can be made from a projection of the cross section of the lens obtained from the binary data onto a plane perpendicular to the (110) direction. Such a projection yielded a value 0.51

---

[17] T. L. Loucks (private communication).

± 0.01 Å^{-1}, which compares quite well with the above caliper.

The maximum dimension of the projection of the lenses centered on L_1 and L_3 was obtained with the magnetic field in the $(\bar{1}10)$ direction. The data indicate $C_{L_1}^{90^\circ}=C_{L_3}^{90^\circ}=1.20\pm0.03$ Å^{-1}. The fact that $C_{L_2}^{0^\circ}$ differs slightly from $C_{L_1}^{90^\circ}$ and $C_{L_3}^{90^\circ}$ is evidence that the lenses are not exactly circular since a circular shape would imply that all three of these dimensions are equal. The minimum dimension $C_{L_1,L_3}^{0^\circ}$ was obtained with the magnetic field in the [001] direction. In this region the data split into two branches yielding two separate values for $C_{L_1,L_3}^{0^\circ}$. One set of data indicated a value of 0.81 ± 0.02 Å^{-1}, while the other set gave a value of 0.83 ± 0.02 Å^{-1}. This split in the data can be attributed to a misalignment of the sample with the sound propagating about 1° off the (110) direction toward the $(\bar{1}10)$ direction.

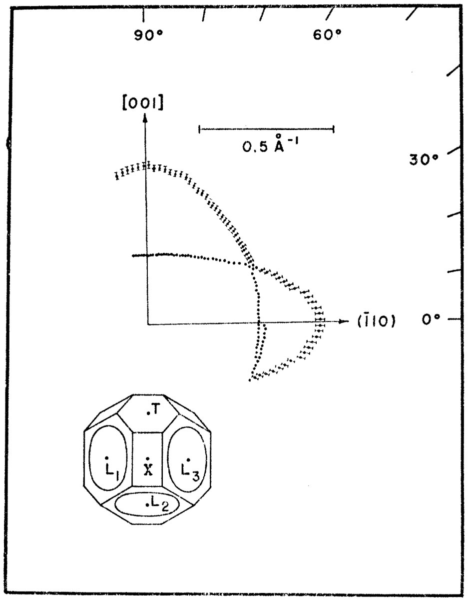

FIG. 4. A polar plot of data with **q** in the (110) direction. A projected view of the Brillouin zone in the (110) direction is shown along with a sketch of the free-electron lenses. The data were taken at a frequency of 135 MHz.

3. Results for **q** *Parallel to the* $(11\bar{2})$ *Direction*

A total of five distinct resonance branches were obtained for **q** parallel to the $(11\bar{2})$ direction and **H** rotated in the $(11\bar{2})$ plane. The two primary branches are shown in a polar plot in Fig. 5 along with a projection of the Brillouin zone onto the $(11\bar{2})$ plane with the free-electron lenses sketched in for comparison. One of these primary branches has been assigned to a projection of the lens centered on L_1 onto the $(11\bar{2})$ plane with the other primary branch being assigned to a similar projection of the lens centered on L_2. Both of these projections should be symmetrical and should intersect at 0° and 90° in the polar representation of Fig. 5 if the crystal is properly oriented. There is no definite evidence of resonances corresponding to calipers of the projection of the third lens centered on L_3. However, the orbits which should give rise to these resonances have a small radius of curvature over the region to be calipered. It has been pointed out[18] that the amplitude of the geometric resonances should depend quite strongly on the radius of curvature of the orbit. Orbits with large radii of curvature should produce larger amplitude resonances than those with small radii of curvature. In light of this fact one expects the signals from the L_3 resonance to be weak.

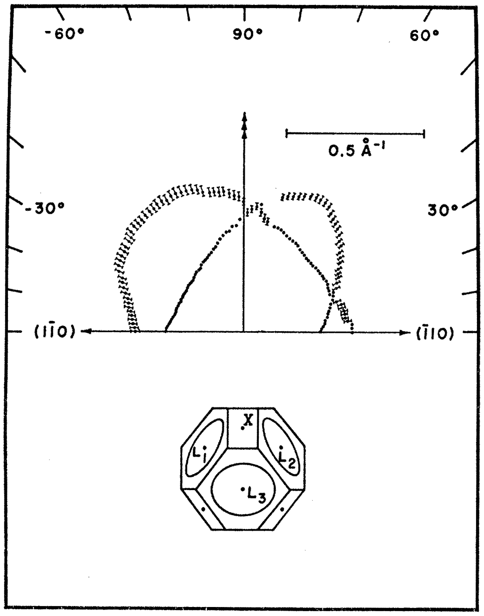

FIG. 5. A polar plot of data with **q** 5° from the $(11\bar{2})$ direction. A projected view of the Brillouin zone in the $(11\bar{2})$ direction is shown along with a sketch of the free-electron lenses. The data were taken at a frequency of 165 MHz.

The crystal from which the data in Fig. 5 was obtained was misoriented with the bisectrix plane rotated about 5 deg about the trigonal axis. This misorientation is readily obvious from the data since the shapes and the areas of the projections of the two lenses, L_1 and L_2, differ considerably. The experimental data indicate that the two projections intersect at polar angles of 20° and 88° instead of 0° and 90°. The minimum C caliper dimension of the L_2 projection was found to be 0.69 ± 0.01 Å^{-1}, while the minimum dimension of the L_1 projection was found to be 0.50 ± 0.01 Å^{-1}. The crystal misalignment consequently accounts for a difference of roughly 39% in the minimum dimensions. In contrast, the maximum diametral dimensions of the two projections agree quite well with the L_2 projection having a dimension of 1.12 ± 0.02 Å^{-1} and the L_1 projection having a dimension of 1.09 ± 0.02 Å^{-1}.

---

[18] S. G. Eckstein (to be published).

4. *Results for* **q** *Parallel to the (100), (111), and [110] Directions*

In addition to the three orientations just discussed, an attempt was made to obtain data on the lens surfaces for **q** directed in the (100), (111), and [110] directions.

The (100) direction is most interesting, since with **H** rotated in the (100) plane one should be able to obtain the main cross section of the lens cut by the (100) face. However, due to the strong open-orbit absorption that exists in this direction, the maximum frequency obtainable was 45 MHz, in which case only a maximum of about two oscillations were observed before the signal saturated. At higher frequencies the signal saturated with no resonances being observed. The lack of amplitude of the lens resonance in this plane could also be attributed to the large curvature of the orbits over the region to be calipered as was the case with the lens centered on L_3 in the $(11\bar{2})$ plane. Thus no additional information was obtained from this orientation.

An attempt was made to propagate the sound along the [110] direction and obtain data for **H** in the [110] plane. This direction is of interest because it would yield the symmetric cross section of the lens cut by the ΓLW plane. This cross section forms, along with the two cross sections from the $(1\bar{1}0)$ and (100) planes, the set of three orthogonal cuts of the lens. A consistency check on the value of $C_{L_2}{}^{0°}$ could have been made, since with **q** parallel to the [110] direction and **H** parallel to the $(11\bar{2})$ direction, the caliper obtained from the lens should be identical to $C_{L_2}{}^{0°}$ obtained from the data with **q** parallel to the (110) direction. This attempt failed as the result of not being able to make a successful acoustic bond between the delay rod and the sample.

With **q** parallel to the (111) direction and **H** rotated in the (111) plane, resonances were observed which corresponded to calipers of the three identical elliptical projections of the electron lens. Since these three sections give rise to resonances all of about the same amplitude with two of the sections, and in some instances all three, having approximately the same caliper value, the additional information obtained from the present data was not of sufficient interest to be reported.

5. *Summary of Electron Data*

In summary, three major symmetry dimensions of the second-zone electrons lens have been determined experimentally. The values obtained are $k_{\text{lens}}{}^{L-\Gamma}=0.176\pm0.004$ Å^{-1}, $k_{\text{lens}}{}^{L-U}=0.538\pm0.010$ Å^{-1}, and $C_{L_2}{}^{0°}=1.28\pm0.03$ Å^{-1} or $k_{\text{lens}}{}^{L-W}=0.64\pm0.015$ Å^{-1}, respectively. The first two dimensions, along with intermediate calipers, give a cross sectional area in the $(1\bar{1}0)$ plane that agrees within 2% of the experimental dHvA data. The remaining dimension, $C_{L_2}{}^{0°}$, gives the maximum diameter of the lens along the $L-W$ line. The fact that the diameters of the lens along $L-U$ and $L-W$, i.e., $2k_{\text{lens}}{}^{L-U}$ and $C_{L_2}{}^{0°}$, differ by about 8% indicates that the lens is not a surface of revolution about the line $\Gamma-L$.

6. *Pseudopotential Coefficients*

The pseudopotential coefficients corresponding to the planes bounding the first Brillouin zone in mercury have been estimated by comparing the geometric resonance data obtained from the lens with the results of a four pseudowave calculation neglecting spin-orbit coupling. Further, there was no attempt to maintain compensation. The Fermi energy as well as the pseudopotential coefficients were treated as adjustable parameters, with the restriction that V_{111} and V_{110} must be equal, as the magnitudes of the (111) and (110) reciprocal lattice vectors differ by less than 0.5%.

The calculation was performed by initially selecting the four plane wave states which had the lowest free-electron energies when restricted to regions near the point of interest. The secular determinant was constructed and a search was performed at a fixed Fermi energy for those values of k which caused the determinant to vanish. The results were subsequently plotted to give profiles of the portion of the Fermi surface under investigation. This procedure was found to be convenient in that calipers not along symmetry lines could be as easily determined as those along lines of high symmetry, and comparison of dHvA areas could also be accomplished.

Since the data for the second-band electron surface is the most reliable, the approach was to first seek agreement between the calculation and this data. The electron surface resembles a deformed lens centered

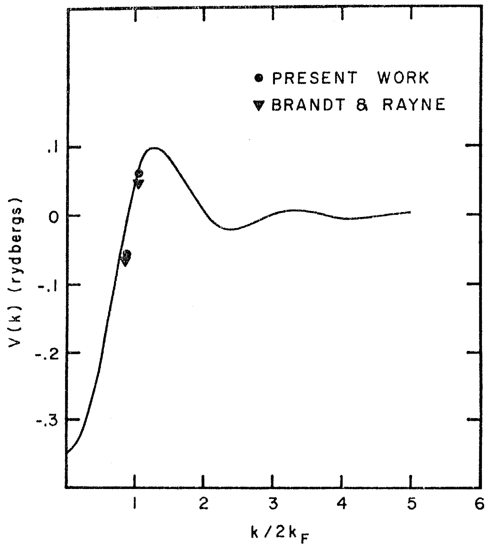

FIG. 6. Pseudopotential for mercury computed by Animalu and Heine with the present calculated values as well as those of Brandt and Rayne shown for comparison. A reduced value of k_F was used which accounts for the fact that the present values are displaced slightly to the right of Brandt and Rayne's.

on the point L, hence it was found convenient to start with only two pseudowaves in the $(1\bar{1}0)$ plane. From this calculation, an initial value of V_{001} was obtained, and a relation between the Fermi energy and the value of V_{001} was established using the experimental results for the minor axis caliper, $k_{\text{lens}}{}^{L-\Gamma}$. A 4 pseudowave (4 PW) calculation was then performed about the point L in the ΓLW plane which allowed the best values for V_{110} and V_{111} to be determined as well as the final value of the Fermi energy which was consistent with the second-band data. The values obtained for the pseudopotential coefficients are $V_{110}=V_{111}=0.0616$ Ry and $V_{100}=-0.0546$ Ry. These values are in reasonable agreement with the work of Animalu and Heine[19] and are compared with their results in Fig. 6. The results of Brandt and Rayne are also shown for comparison. The results of the calculation for the $(1\bar{1}0)$ cross section are shown in Fig. 7 compared to the data. It should be noted that the 4 PW method yields reasonable agreement with the data if the Fermi level is depressed to 0.505 Ry, about 4.0% below the free-electron value. The dHvA area for the $(1\bar{1}0)$ cross section of the electron surface and that indicated by the present measurements are in excellent agreement, both with each other and the present 4PW results.

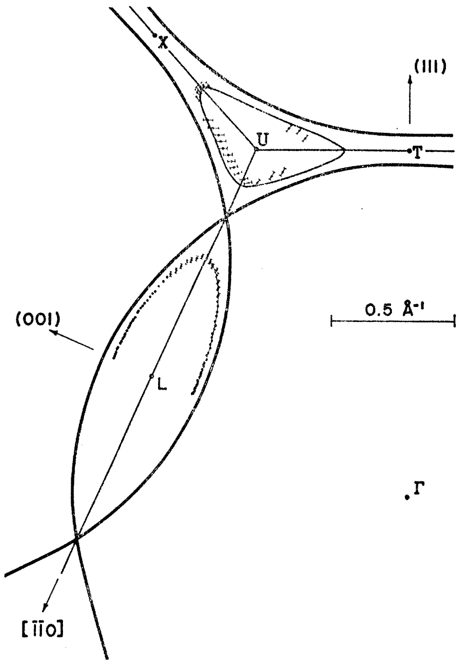

FIG. 7. A plot of the experimental data in the $(1\bar{1}0)$ cross section of the Fermi surface compared with the free-electron surface and the results of a 4PW calculation. The thick lines indicate the free-electron surface. The τ section indicated by the solid line and centered on U is the result of the present calculation as is the section indicated by the thin line overlying the data centered on L.

TABLE III. Comparison of radii of openings in first-zone hole surface. Values are in Å^{-1}.

Model	$k_{\text{in}}{}^{L-U}$	$k_{\text{in}}{}^{X-U}$	$k_{\text{in}}{}^{T-U}$	$k_{\text{in}}{}^{T-W}$	$k_{\text{in}}{}^{X-K}$
RAPW[a]	0.948	0.117	0.117[b]	0.117[b]	0.115
HAA[a]	0.831	0.354	0.382[b]	0.382[b]	0.347
MAG V[a]	0.860	0.260	0.198[b]	0.198[b]	0.209
8 PW[a]	0.874	0.177	0.071[b]	0.071[b]	0.209
dHvA 3PW[a]	0.897	0.299	0.324[b]	0.324[b]	0.182
Present calculation	0.870	0.300	0.270	0.340	0.185
Present experiment	0.90	0.30			

[a] See Ref. 5.
[b] Circular approximation.

The calculation was then extended to allow determination of the orbit shapes along various symmetry lines. Experimental and present theoretical results were compared at several points of interest in the zone and are summarized in Tables II–IV. A survey of the results of the calculation shows general agreement with the topological features of the Fermi surface of mercury as suggested by other workers as well as by the present experiment; however, there remains need for improvement. Indeed, the present calculation is not presented as a substitute for a rigorous band calculation, but only as a method by which some of the available experimental data may be compared.

The 4PW results, along with other existing calculations, will be compared to the data from the hole surface in the following section. Further, the 4PW calculation will allow some extrapolation of the experimental results to calipers not directly observed. The present theory is fit to the electron surface, as opposed to the method of earlier workers. Thus it is to be expected that the largest discrepancies between theory and experiment will be found for the smaller orbits on the hole surface such as the β orbits which will be discussed later. As will be evidenced in Sec. V B, the larger hole-surface calipers in general show better agreement between the present calculation and experiment than do those due to the smaller sections of the hole surface.

B. Hole Surface

1. *Results for* q *Parallel to the* $(1\bar{1}0)$ *Direction*

The resonance branches designated by β, ϵ_1, ϵ_2, δ, γ, μ_1, μ_2, and η shown in Fig. 2 have all been assigned to C calipers associated with various orbits on the first-zone hole surface. A representation of this surface

TABLE IV. Comparison of outside dimensions of the τ section as measured from L, T, and X. Values are given in Å^{-1}.

Method	$k_{\text{out}}{}^{L-U}$	$k_{\text{out}}{}^{T-U}$	$k_{\text{out}}{}^{X-U}$	$k_{\text{out}}{}^{T-W}$
dHvA 3PW[a]	1.16	0.78	0.765	0.935
Present calculation	1.18	0.79	0.79	1.00
Present experiment	1.14	0.77	0.765	0.90

[a] See Ref. 1.

---

[19] A. O. Animalu and V. Heine, Phil. Mag. **12**, 1249 (1965).

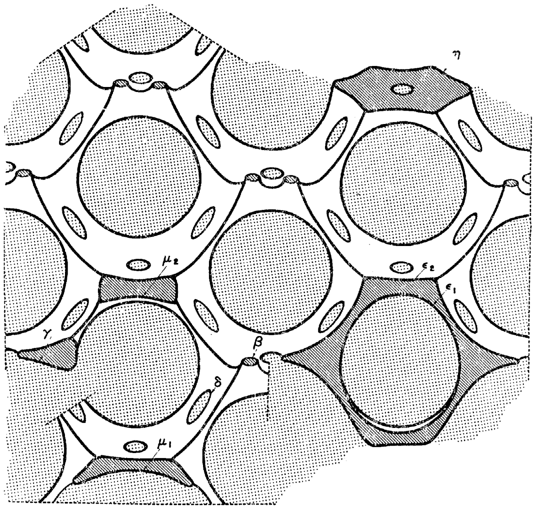

FIG. 8. A representation of the first-zone hole surface in mercury in the extended zone scheme. The experimentally observed orbits are indicated with Greek letters.

along with the labeled orbits is shown in Fig. 8. Among the more interesting orbits from this set are those designated by ϵ_1, ϵ_2, δ, and η. The branch denoted by ϵ_1 has been assigned as the caliper of an orbit centered on L around the inside of the hole surface with H in the vicinity of the (001) direction. This orbit was observed over a range of about 6° and yielded a radial caliper that varied from 0.91 ± 0.02 to 1.03 ± 0.02 Å^{-1}. The branch denoted by ϵ_2 has been assigned to an orbit lying in the same plane as ϵ_1, but moving on the outside of the hole surface and threading through the openings in the T faces. This orbit was observed over the same range as ϵ_1 and yielded a radial caliper that varied from 1.16 ± 0.02 to 1.18 ± 0.02 Å^{-1}.

The η branch has been assigned to a hexagonal shaped orbit centered at T completely enclosing the T face which occurs when the magnetic field is directed in the vicinity of the trigonal axis. This orbit was observed over an angular range of about 12° on either side of the (111) direction and gave radial calipers that varied from a maximum of 0.83 ± 0.02 Å^{-1} to a minimum value of 0.66 ± 0.02 Å^{-1} with the field tilted 12° toward [001]. The radial caliper obtained with the field along the (111) direction was 0.77 ± 0.02 Å^{-1}.

The δ branch has been assigned to an orbit on the inside of the opening on the X face centered on the point X. This orbit was observed with the magnetic field in the vicinity of the (110) direction and was detectable over a range of approximately 8° on either side of the (110) direction giving a radial caliper of 0.30 ± 0.01 Å^{-1} for this particular direction. The data obtained from the orbits are plotted in the $(1\bar{1}0)$ plane in Fig. 7 along with the α_1 data for comparison. Note that calipers obtained from ϵ_1, ϵ_2, η, and δ almost completely determine the cross section of the hole surface centered on U. This cross section corresponds to the area enclosed by the τ orbit of Brandt and Rayne. The cross section generated by the τ orbit will be referred to as the τ section.

The results of the 4PW calculation in the $(1\bar{1}0)$ plane based on the present data are shown in Fig. 7. As is evident, the fit to the lens section is extremely good with the extremal dimensions and enclosed area agreeing within experimental error. The fit to the τ section is fairly good with the calculation lying for the most part slightly outside the experimental data. It should be noted that most of the experimental data assigned to the τ section was taken from orbits with rather large dimensions. Thus errors in determining the dimensions of these orbits imply large errors on the small scale of the τ section. The area of the τ section has been determined from the present calculation and found to be 0.132 Å^{-2}. This is considerably smaller than the experimental dHvA area of 0.151 Å^{-2}, but agrees with the RAPW calculation of 0.132 Å^{-2}. The dHvA 3PW calculation gives a value of 0.107 Å^{-2} while the 8PW calculation yields a value of 0.151 Å^{-2} in agreement with the experimental dHvA data. It is to be noted that while the 8PW calculation fits the dHvA experimental data for the τ section, it is in disagreement with the corresponding experimental area for the $(1\bar{1}0)$ lens section by about 27%, giving a value of 0.423 Å^{-2} as compared to the experimental area of 0.305 Å^{-2}. The present calculation gives good agreement for the area of the lens but is in disagreement with the measured dHvA area of the τ section by about 15%.

There are several important dimensions that can be obtained from a knowledge of the τ section. These include the width of the openings in the X, T, and L faces. Figure 9 indicates these dimensions along with

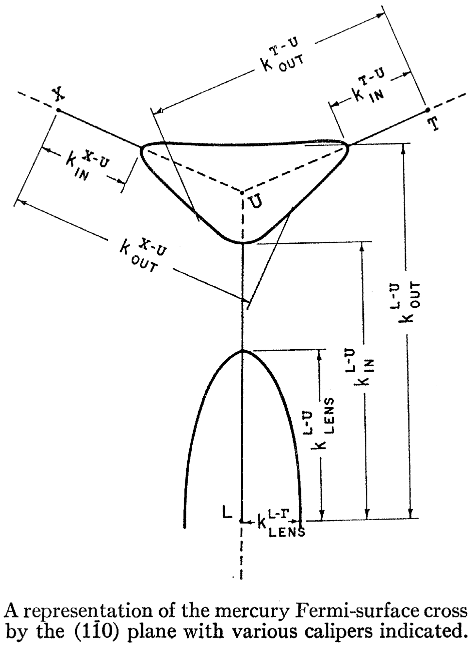

FIG. 9. A representation of the mercury Fermi-surface cross section by the $(1\bar{1}0)$ plane with various calipers indicated.

the corresponding notation while the values are given in Table III. Data obtained from the δ orbit with the magnetic field in the (110) direction yield a value for the major dimension of the opening in the X face of $k_{\text{in}}{}^{X-U}=0.30\pm0.01$ Å^{-1} which is precisely the same value obtained from the 4PW calculation. The dimensions of the opening in the T face were determined exclusively from the 4PW calculation since ultrasonic data could not be obtained for this direction. The lack of data from orbits from which the size of the opening could be determined was due to the fact that resonances from the lens and η orbits completely dominated the attenuation and consequently obscured weaker resonances. The calculation indicates a minimum value for the width of the opening of $k_{\text{in}}{}^{T-U}=0.27$ Å^{-1} and a maximum width of $k_{\text{in}}{}^{T-W}=0.340$ Å^{-1}. A circular approximation to the opening has been made in the 8PW calculation and gives a value of $k_{\text{in}}{}^{T-U}=k_{\text{in}}{}^{T-W}=0.071$ Å^{-1}, while the dHvA 3PW calculation gives a result of 0.324 Å^{-1} for the same dimension also in a circular approximation. The width of the opening in the L face should be measured directly from the ϵ_1 orbits. However, this opening can be better defined from the η orbit centered on T as is evident from Fig. 7. The data indicate a value of $k_{\text{in}}{}^{L-U}=0.90\pm0.02$ Å^{-1} as compared to a calculated 4PW value of $k_{\text{in}}{}^{L-U}=0.870$ Å^{-1}. A comparison of the various breakthrough dimensions on the hole surface as determined by different methods is given in Table III.

Three other dimensions that can be determined from the experimental data are the outside calipers of the τ section measured from the points X, T, and L. These calipers are denoted as $k_{\text{out}}{}^{X-U}$, $k_{\text{out}}{}^{T-U}$, and $k_{\text{out}}{}^{L-U}$ as indicated in Fig. 9. The experimental results are tabulated in Table IV along with the corresponding 4*PW* and dHvA 3PW dimensions for comparison. The dimension $k_{\text{out}}{}^{T-U}$ was determined directly from the η orbits while $k_{\text{out}}{}^{X-U}$ was determined indirectly from the ϵ_1 orbits. The experimental determination of $k_{\text{out}}{}^{L-U}$ utilizes the dimension $C_\tau{}^{L-U}$ as explained later in this text.

The calipers designated β have been assigned to orbits around the arms on the hole surface extending along the $\langle 100\rangle$ directions as indicated in Fig. 8. Resonances corresponding to these calipers were observed over an angular range of about 18° and gave a value of 0.065 ± 0.010 Å^{-1}. The minimum caliper should occur with the magnetic field directed along the [100] direction, but unfortunately the β resonances were obscured about 8° from this point. The dHvA 3PW calculation indicates a minimum caliper in a circular approximation of approximately 0.04 Å^{-1} while the present calculation gives a value of 0.06 Å^{-1}. It might be pointed out that dHvA type of oscillations have been observed in the acoustic attenuation with the magnetic field in the range of 7 to 12 kG in a separate oblique field experiment. These oscillations give areas assignable to the β orbits which agree with the data of Brandt and Rayne.

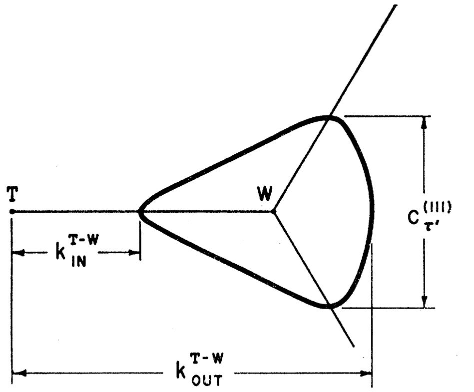

FIG. 10. A representation of the τ' hole orbit with corresponding notation indicated.

The calipers denoted by γ were assigned to an orbit that passes through the opening in the T face as illustrated in Fig. 8. Experimentally this orbit was observed over a range of approximately 40° giving C calipers that varied from 0.38 ± 0.04 to 0.58 ± 0.04 Å^{-1}. When the magnetic field is in the $(11\bar{2})$ direction, the γ orbit will be referred to as a τ' orbit, in which case the height of the orbit denoted $C_{\tau'}{}^{(111)}$ in Fig. 10 was found to be 0.475 ± 0.04 Å^{-1} as compared to the 4PW value of 0.520 Å^{-1} and a dHvA 3PW value of 0.420 Å^{-1}.

The two remaining resonance branches in the $(1\bar{1}0)$ plane have been assigned to calipers associated with orbits μ_1 and μ_2, with μ_1 being first proposed by Keeton and Loucks.[6] μ_1 was observed over a range of approximately 30° with C caliper values ranging from a minimum of 0.200 ± 0.020 Å^{-1} to a maximum of 0.440 ± 0.040 Å^{-1}. With the magnetic field in the (001) direction the C caliper obtained for the μ_1 orbit will closely match the diametral caliper of the τ section along the $L-U$ line. This dimension is denoted as $C_\tau{}^{L-U}$, and it can be seen from Fig. 9 that $k_{\text{out}}{}^{L-U}=k_{\text{in}}{}^{L-U}+C_\tau{}^{L-U}$. The experimental data indicate a value of $C_\tau{}^{L-U}$ of 0.240 ± 0.020 Å^{-1} as compared to the dHvA 3PW value of 0.260 Å^{-1} and a value of 0.31 Å^{-1} obtained from the present 4PW calculation. Using the values of $C_\tau{}^{L-U}$ and $k_{\text{in}}{}^{L-U}$ determined experimentally, then $k_{\text{out}}{}^{L-U}=1.14$ Å^{-1} is obtained which is in reasonable agreement with the present calculated value of 1.18 Å^{-1}. The resonance branch μ_2 has been assigned to a "bowtie orbit" as indicated in Fig. 8. This orbit was observed over an angular range of 10° with C calipers ranging from 0.258 ± 0.020 to 0.166 ± 0.020 Å^{-1}.

The present calculation for the width of the openings in the T and X faces indicate that the $\mathbf{H}\|(1\bar{1}0)$ direction open orbit, first observed by Dishman and Rayne,[5] can exist. It was impossible to detect any resonance due to this open orbit since the attenuation at fields corresponding to low integer values of the open orbit resonance was very high.

2. *Results for* q *Parallel to the* $(11\bar{2})$ *Direction*

Three resonance branches were observed in this direction which could be assigned to orbits on the hole surface. There was considerable evidence for the existence of the β orbits with the data indicating radial calipers that ranged from a minimum of 0.08 ± 0.01 Å^{-1} to a maximum of 0.181 ± 0.020 Å^{-1}. With the magnetic field in the $(11\bar{2})$ plane, a direction was never assumed for which the minimum radial caliper of the β orbit could be obtained. As was pointed out earlier, the minimum radial caliper for this orbit should be approximately 0.06 Å^{-1}.

With the magnetic field in the vicinity of the (111) direction there was strong evidence of the η orbit discussed previously. This orbit was observed over an interval of 10° and gave a radial caliper of $k_{\text{out}}^{T-W} = 0.90\pm0.02$ Å^{-1} with **H** in the (111) direction. The dHvA 3PW calculation gives 0.93 Å^{-1} while the present 4PW calculation gives a value of 1.00 Å^{-1} for the same dimension.

The third resonance branch was observed with the magnetic field in the vicinity of the $(1\bar{1}0)$ direction yielding calipers in the region of the intersection of the L_1 and L_2 projections of Fig. 5. The data in this area were very difficult to analyze due to the complicated mixing of three or more periods. It was almost impossible to resolve more than one period with any accuracy. With the magnetic field in the region from 4° to approximately 16° from the $(1\bar{1}0)$ direction, the dominant resonance yielded C caliper values that ranged from 1.02 ± 0.02 to 1.20 ± 0.03 Å^{-1}, too large to be associated with the L_1 or L_2 projections. It is possible that these calipers might be assigned to the open orbit that exists with the field in the $(1\bar{1}0)$ direction. Ideally, the caliper of the open orbit should give a value equivalent to $\frac{1}{3}$ the zone height or 0.943 Å^{-1}. However, it could be possible to obtain a larger value as a result of the misorientation of the crystal.

3. *Summary of Hole Results*

The primary information obtained from the various hole orbit calipers was a description of the τ section in the $(1\bar{1}0)$ plane along with several breakthrough dimensions on the hole surface. The data for the τ section is in general agreement with the results of a 4PW calculation although the calculated area is still about 15% too small to agree with the experimental dHvA data. In order to fit the dHvA area of Brandt and Rayne, a breakthrough dimension in the T face much smaller than that predicted from the present 4PW calculation is required. The 8PW approach of Dishman and Rayne predicts such a dimension, i.e., 0.071 Å^{-1}. However, as discussed by Dishman and Rayne, a breakthrough dimension of this size in the T face is not compatible with their magnetoresistance open orbit data. In view of this there is still need for a further determination, both experimentally and theoretically, of the τ cross section and in particular the dimension k_{in}^{T-U}. The agreement between the remaining breakthrough dimensions determined experimentally from the hole orbits and those calculated using the 4PW method is generally less satisfactory than the agreement between the 4PW calculation and the electron surface data wherever such comparisons can be made.

VI. CONCLUSION

The results of this investigation indicate that the Fermi surface of mercury consists of three electron lens belonging to the second-zone and a multiply connected first-zone hole surface. This agrees with the model that has been previously proposed. The hole surface has been found to contact all faces of the Brillouin zone producing breakthrough regions or openings in the surface. The 4PW calculation performed is in general agreement with the data obtained from both the electron and hole surface. It should be noted, however, that this calculation is not found to be superior to previous calculations. Rather, it suggests that no better fit to the available data for the Fermi surface can be obtained by choosing pseudopotential coefficients to fit only the electron data than was found by previous workers when they fit only the hole-surface data. For example, the 4PW calculation was fit to the experimental data on the second-band electron surface and the resulting hole surface was also generated. Consequently, the fit to the electron surface was extremely good but the agreement with the β and τ orbit data was not as satisfactory. The dHvA 3PW RAPW calculations which placed emphasis on fitting the dHvA data to the hole surface, in particular to the β orbit, both give a τ section comparable with that of the present data. However, both differ markedly from the experimental dHvA data on the τ section, and with the electron-surface data of both the dHvA and the present experiment. The 8PW calculation, on the other hand, fits the τ section as well as the β section to the dHvA data exactly, but in the process worsens the disagreement between the area of the electron section and the corresponding experimental data as well as conflicting with the open orbit data.

It would appear, therefore, that there is need for further detailed calculations to resolve the apparent discrepancies between the existing experimental and theoretical results.